Influence of Laser Processing Strategy and Remelting on Surface Structure and Porosity Development during Selective Laser Melting of a Metallic Material

CHUNLEI QIU, ZHUO WANG, AIMAN SALIM ALADAWI, MOHAMMED AL KINDI, ISSA AL HATMI, HU CHEN, and LEI CHEN

316L samples were fabricated by selective laser melting (SLM) with different laser powers and scanning strategies/patterns. The porosity distribution and surface structures of the as-fabricated samples were characterized using optical microscopy and scanning electron microscopy. This combined with a mathematical modeling of the SLM process aims to understand the formation mechanism of pores in a newly built layer and the role of remelting of previous layers on internal porosity development. It is shown that the surface structure and the formation of pores in a newly built layer are mainly associated with melt flow behavior, but the formation of pores within bulk samples, particularly those at interlayer interfaces, were largely dictated by the extent of remelting of previous layers during SLM. Laser melting of a powder layer tends to develop rough surfaces and open pores on the uppermost layer. With laser remelting of a newly built layer, the sample surfaces become much smoother and the pores within the uppermost layer can be completely eliminated. During SLM processing, sufficient remelting of previous layers leads to development of good bonding at the interlayer interfaces, whereas less extent of remelting of previous layers results in an increased number of pores at the interlayer interfaces. Laser power or energy density shows a much more dominant role than the laser scanning strategy in porosity development, which is attributed to the fact that laser power or energy density shows greater influence on the extent of remelting as compared with the latter. The mechanism on how remelting affects the evolution of pores is also demonstrated through modeling.

https://doi.org/10.1007/s11661-019-05348-0

I. INTRODUCTION

ADDITIVE manufacturing technologies, such as selective laser melting (SLM) and direct laser deposition (DLD), are increasingly used to fabricate components for various applications due to their excellent near-net-shape manufacturing capacity. These technologies show unique processing characteristics such as layerwise manufacturing, complex laser-material interaction, melting of powder layers and remelting of previous layers, high thermal gradient in melt pools and thus tendency for directional solidification, rapid solidification, and cooling. The first three characteristics greatly influence the inter-layer bonding, surface structure, and porosity development in as-fabricated samples, while the rest show great influence on microstructural development. Given that both defects (such as porosity) and microstructure can greatly affect the mechanical properties of additively manufactured materials, considerable studies have been conducted on additively manufactured metallic materials to minimize defects and optimize microstructure as well as to develop understanding on the formation mechanism of defects and microstructure during SLM and DLD.

Regarding the mechanism of formation of pores during SLM, Qiu *et al.*[1] and King *et al.*[2,3] first investigated the interaction between a laser heat source and a powder layer through both the modeling

CHUNLEI QIU is with the School of Materials Science and Engineering, Beijing University, Beijing, 100083, P.R. China, and also with the School of Engineering, Cardiff University, The Parade, Cardiff, CF24 3AA, UK. Contact email: chunlei_qiu@buaa.edu.cn ZHUO WANG and LEI CHEN are with the Department of Mechanical Engineering, Mississippi State University, Starkville, MS 39762. AIMAN SALIM ALADAWI, MOHAMMED AL KINDI, and ISSA AL HATMI are with the School of Engineering, Cardiff University. HU CHEN is with the Department of Mechanical Engineering, Mississippi State University, and also with the School of Materials Science and Engineering, Tsinghua University, Beijing 100084, P.R. China.

Manuscript submitted October 30, 2018.
Article published online July 8, 2019

approach and experimental observation and revealed that unstable melt flow plays a major role in the formation of pores in a freshly melted layer and in surface structure development. Unstable melt flow tends to lead to melt splashing and to the development of increased porosity and irregularly shaped surface structure on the newly built layer.[1] The melt flow behavior during SLM was further *in situ* investigated by Leung *et al*.[4] and Zhao *et al*. recently[5] using high speed X-ray imaging. Leung *et al*. directly observed that the laser-induced gas/vapor jet promotes the formation of melt tracks and denuded zones *via* spattering. They also demonstrated the pore migration by Marangoni-driven flow and pore dissolution and dispersion by laser remelting. Zhao *et al*. demonstrated that where local input energy density is too high, the melt pool would become deep and the melt flow so unstable that keyhole pores would be developed. This is consistent with Qiu *et al*.'s work[6] on SLM-processed Invar 36, where they observed that under certain processing conditions, the laser is so powerful that it can penetrate down through many previous layers and create a deep melt pool, and when the laser is moved away, a keyhole pore forms at the bottom. These studies greatly improve understanding on melt flow behavior during SLM and its role in the formation and evolution of pores, particularly those pores formed in a newly melted layer. However, the pore development in a newly melted layer does not necessarily represent that in a bulk sample, because during continuous multiple layer additive manufacturing, laser remelting of previous layers may have great influence on pores developed in previous layers or at interlayer interfaces. When the laser input energy is high and the extent of laser remelting of previous layers sufficient, the pores present in the previous layers stand a good chance of being eliminated. This is evidenced by Yasa *et al*.'s work,[7] where laser remelting was performed on each freshly melted and consolidated layer during SLM and was found to be effective in reducing porosity within bulk samples. It is also known that when there is a serious lack of fusion at the interlayer interfaces, *i.e*., lack of remelting of previous layer, elongated pores (or so-called lack-of-fusion pores) can form, which usually lead to mechanical property anisotropy.[6,8] It is therefore necessary to investigate the influence of the extent of remelting of the previous layer on the size, morphology, and distribution of pores within bulk samples with the aim of developing control of the porosity level within additively manufactured samples. In this study, a series of laser processing conditions, such as laser powers, will be used to process a common metallic material 316L to investigate the influence of the extent of remelting of previous layers on porosity development during SLM. Direct laser remelting on some newly built layers will also be conducted to understand its influence on surface structure and porosity development. Mathematic modeling will be developed to understand the evolution mechanisms of those pores that already exist in previous solidified layers during laser remelting.

Moreover, it is noted that the current AM processes usually offer a number of processing variables to investigate. These include laser power, laser scanning speed, powder layer thickness, laser scanning strategy, hatch spacing, and laser mode. From the industrial manufacturing point of view, it is important to identify some of the most important parameters that dictate the development of defects and microstructure so that researchers can simply focus on these several parameters instead of investigating all the processing variables to achieve the desired density and microstructure and required mechanical properties. So far, there are separate studies on the influence of the processing condition (such as laser power, scanning speed, and powder layer thickness)[9–15] or laser scanning strategy[16–19] (such as laser scanning/hatching patterns, hatching spacing, and laser mode) on the porosity and microstructure of different metallic materials, but systematic study to determine which factor (between the processing condition and laser scanning strategy) dominates porosity and microstructural development of a metallic material during SLM is still lacking. Thijs *et al*.[17] conducted an investigation of the influence of laser processing parameters (such as laser scanning speed and hatching spacing) on the porosity and grain structure under several different laser scanning patterns but did not determine which factor (between processing condition and laser scanning strategy) plays a more important role in porosity development. Therefore, another emphasis of this study is to identify the most important processing variable for porosity development during SLM by conducting a comparative study on the influence of the laser processing condition and that of the laser scanning strategy on porosity based on 316L stainless steel. The influence of the laser processing condition and scanning strategy on microstructural and mechanical property development is reported elsewhere.[20]

In general, the aim of the current study is to determine the influence of the extent of remelting of the previous layer on porosity development and the evolution mechanism of pores during laser remelting. Another major goal is to identify the most influential processing parameter that could dominate the extent of remelting of the previous layer and porosity development.

II. EXPERIMENTAL AND MODELING METHODS

A. *Experimental*

The material used in this study is gas-atomized 316L powder supplied by Renishaw plc (Wotton-under-Edge) in the size range of 15 to 45 μm. The chemical composition of the as-received powder is summarized in Table I. A Renishaw 250 SLM system, which employs a fiber laser with a maximum power of 200 W, was used to prepare samples with a dimension of $10 \times 10 \times 12$ mm^3 for microstructural characterization. The samples were fabricated in an argon atmosphere with different laser scanning strategies, including Meander, Stripe, and Chessboard scanning strategies (illustrated in Figure 1), or with different laser powers, including 110, 140, 170, and 200 W. Among all the scanning strategies, the Chessboard scanning strategy

Table I. Chemical Composition of As-Received 316L Stainless Steel Powder (Weight Percent)

Element	Ni	Cr	Mo	Mn	Cu	Si	S	O	C	Fe
Wt Pct	12.5 to 13	17.5 to 18	2.25 to 2.5	2	0.5	0.75	0.01	0.10	0.03	bal.

Fig. 1—Schematic illustration showing the laser scanning strategies used in the current study: (*a*) Meander, (*b*) Stripes, and (*c*) Chessboard (Reprinted with permission from Ref. 20).

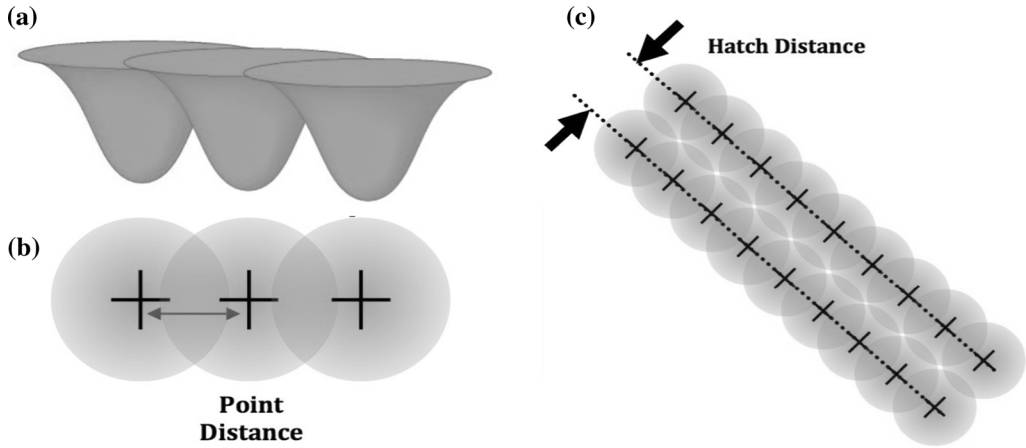

Fig. 2—Schematic illustration showing (*a*) the pulsed laser melting process and the definition of key physical parameters such as (*b*) point distance and (*c*) hatch distance.

divides each layer into a number of square islands that are then randomly scanned by laser afterward. Two island sizes 1×1 mm^2 and 5×5 mm^2 were used in this study. The stripe width for the Stripe scanning strategy was set to 5 mm. Once the hatch scanning was completed on a cross section, a contour scan was performed around the edges of the section. The distance between the hatch boundary and the contour was set as 60 μm.

A pulsed laser mode, where the laser operates by using discrete point exposures instead of running continuously, was used. Each exposure creates a melt pool of metal that takes the form of a three-dimensional Gaussian curve, as shown in Figure 2(a). The laser beam diameter used was around 75 μm and the exposure time for each pulse was 80 μs. Laser melting was performed by radiating discrete and partially overlapped laser spots. The spacing between the central points of two neighboring laser spots (or point distance shown in Figure 2(b)) was set as 60 μm. The speed of laser moving from one exposure to another was set as 5000 mm/s for all the sample fabrications. At the end of each scan line, the laser jumped to a partially overlapped adjacent track. The spacing between the central lines of two neighboring laser scanning tracks, *i.e.*, the hatch distance as shown in Figure 2(c), was defined as 110 μm. The samples were fabricated layer after layer with a powder layer thickness of 50 μm. The scanning direction was rotated 67 deg after each layer so that the same pattern would be repeated every 180 layers. This is believed to be helpful in removing defects such as open pores created in previous layers. The energy density (E) is defined as follows:

$$E = \frac{P * t}{d_h * d_p * l} \quad [\mathrm{J/mm^3}]$$

where P is the laser power, t is the exposure time, d_h is the hatch distance, d_p is the point distance, and l is the powder layer thickness.

The as-fabricated samples were ground using SiC wheels from 200 to 4000 grit before being polished using 3-μm diamond suspension and then colloidal silica suspension (or OPS solution). The samples were then examined using a Nikon optical microscope (OM), which has the capacity to image a 10×10 mm^2 section from a sample. Two complete longitudinal sections from each sample were imaged to develop the distribution of pores for quantitative analysis. The porosity level is quantified as the area fractions of pores on each section (A_f) by using Image J. To investigate the locations of pores in the as-fabricated samples, the as-polished samples were further electrolytically etched in a solution that contains 10 g oxalic acid and 100 mL water prior to microstructural characterization using an OM and scanning electron microscope (SEM).

B. *Modeling*

To numerically investigate the role of remelting in porosity development during SLM, a laminar two-phase flow model coupled with the moving mesh and phase field is employed to capture the interaction between the liquid phase and pore phase in a remelted pool. Regarding the pore phase, two types of pores are assumed in the current modeling: vacuum pores due to shrinkage during solidification and gas pores due to unstable melt flow behavior and gas entrapment. Given that the current SLM was conducted in argon atmosphere, most of the pores formed during SLM may more or less contain some argon. Because of these, it is reasonable to consider two extreme conditions for modeling: vacuum pores and pores containing a high level of argon so that their internal pressure can reach the argon pressure within the processing chamber, in this case 1 atm. The moving mesh and phase field are common interface tracking methods, accounting for differences in density and viscosity of the two phases, as well as surface tension and gravity. The main difference lies in that the moving-mesh method has a more accurate representation of interface without supporting topological changes such as bubble merging. Therefore, the vacuum pores due to shrinkage are handled by the moving mesh, while the phase-field method is used to simulate the gas-induced pore behavior, which may involve pore merging. The liquid is assumed to be incompressible fluid and the compressibility of the pores is considered by using low Mach numbers, Ma < 0.3.[21] As an approximation, the remelt pool is simulated by a parabolic function on the basis of experimental observations. In order to rationalize the evolution of pores during remelting, the coupling of the Navier–Stokes equation (momentum conservation) and continuity equation (mass conservation) needs to be solved:[22]

$$\rho\frac{\partial u}{\partial t}+\rho(\boldsymbol{u}\cdot\nabla)\boldsymbol{u}=-\nabla\cdot\left[-p\boldsymbol{I}+\mu\left(\nabla\boldsymbol{u}+(\nabla\boldsymbol{u})^{T}\right)-\frac{2}{3}\mu(\nabla\cdot\boldsymbol{u})\mathbf{I}\right]+\rho\boldsymbol{g}+\boldsymbol{F}_{\mathrm{ST}}+\boldsymbol{F}_{\mathrm{T}}$$

$$\frac{\partial\rho}{\partial t}+\nabla\cdot(\rho\boldsymbol{u})=0$$

where ρ is the fluid density, p is the fluid pressure, $\boldsymbol{u}$ is the fluid velocity, μ is the fluid dynamic viscosity, and $\boldsymbol{I}$ is the identity tensor. $\rho\mathbf{g}$ is the gravity force, and $\boldsymbol{F}_{\mathrm{ST}}$ represents the surface tension force acting at the interface between the two fluids. $\boldsymbol{F}_{\mathrm{T}}$ accounts for thermally induced thermocapillary force, and a high thermal gradient ($\sim 10^6$ K/m) directed from the top center of the pool to its bottom is applied in the current modeling. In moving mesh, the interface is tracked by the Arbitrary Lagrangian Eulerian method, in which a material interface can be retained when the mesh is deformed properly.[23] Specifically, the Winslow smoothing method is selected for the moving mesh. The moving mesh application mode thus solves the system of partial differential equations below for the mesh displacement:

$$\frac{\partial^2 X}{\partial^2 x}+\frac{\partial^2 X}{\partial^2 y}=0$$

$$\frac{\partial^2 Y}{\partial^2 x}+\frac{\partial^2 Y}{\partial^2 y}=0$$

where x and y are the spatial coordinates of the spatial frame and X and Y are the reference coordinates of the material frame.

The evolution of the interface in the phase field is captured by the convective Cahn–Hilliard equation, in which interfacial diffusion fluxes are assumed proportional to gradients of chemical potential, Ψ:[24]

$$\frac{\partial\phi}{\partial t}+\boldsymbol{u}\cdot\nabla\phi=\nabla\cdot(M(\phi)\nabla\Psi)$$

where $\boldsymbol{u}$ is the bulk velocity, $M(\phi)$ is the phase-field-dependent non-negative mobility, and ϕ is the phase field and is defined as the difference between the concentrations of the two mixtures[25]

$$\phi=\frac{m_1-m_2}{m_1+m_2}$$

where m_1 and m_2 are the masses of fluids 1 and 2 and thus $-1\le\phi\le 1$.

The chemical potential, Ψ, is expressed as

$$\Psi=-\nabla\cdot\nabla\phi+(\phi^2-1)\phi$$

In order to balance the volume difference introduced by the pore shrinkage, the neutral condition is set up as ambient pressure, P_0, on the top boundary:

$$\boldsymbol{n}^{T}\left[-p\boldsymbol{I}+\mu\left(\nabla\boldsymbol{u}+(\nabla\boldsymbol{u})^{T}\right)-\frac{2}{3}\mu(\nabla\boldsymbol{u})\boldsymbol{I}\right]\boldsymbol{n}=-p_0$$

which implies an open boundary allowing two-way flow once volume changes. The other boundaries are set up by the nonslip condition $\boldsymbol{u}=0$.

The preceding equations were solved in two dimensions by using COMSOL Multiphysics software. In simulating the gas-entrapped pores, a time-step of 1×10^{-6} seconds and a mesh density of level "finer,"[26] *i.e.*, 17,000 elements with an element size of 1.25 μm based on the current 420 × 300 μm^2, were used. As a result, each simulation took 5 to 6 hours of computing time based on the Intel XeonÒ CPU E5-2660. For the vacuum pores, a much smaller time-step of 1×10^{-8} s was used to capture the quick filling-up. The meshing remains the same and each simulation takes around 30 minutes.

III. RESULTS

A. *Porosity, Surface Structure, and Solidified Melt Pools*

Figure 3 shows the variation of pores in as-fabricated samples with different laser scanning strategies and laser powers. It is clear that the laser scanning strategy shows a certain influence of porosity in the laser-processed samples but it is not dominant. Actually, the as-fabricated samples show nearly comparable porosity levels. The sample fabricated with the Chessboard scanning strategy with an island size of 1 × 1 mm^2 shows the highest porosity level among all these samples, but its porosity level of 0.61 pct is still low. In contrast to the laser scanning strategy, laser power obviously shows much more pronounced influence on porosity. The porosity level decreases exponentially with increased laser power (from 110 to 200 W), while the size of pores increases continuously with decreased laser power. Their morphology becomes increasingly irregularly shaped (*i.e.*, more elongated or polygonal) according to our previous study.[20] The results suggest that laser power is more of a determining factor in the porosity development of 316L samples than the laser scanning strategy during SLM.

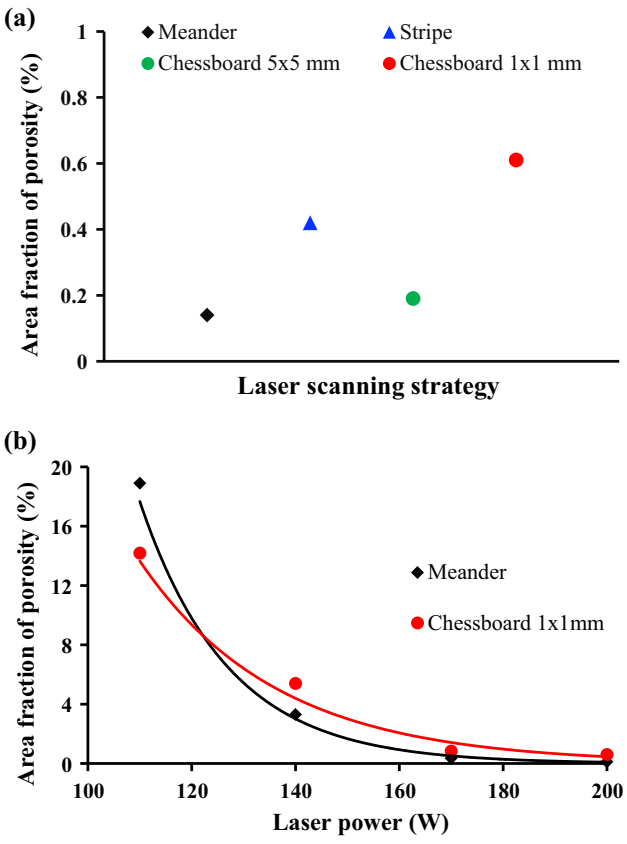

Fig. 3—Variation of porosity level with (*a*) laser scanning strategy and (*b*) laser power (reprinted from Ref. 20 under creative common license, https://creativecommons.org/licenses/by/4.0/).

Given that porosity development is believed to be highly associated with surface structure, which is a direct result of melt flow behaviour,[1] the surface structures of the as-fabricated samples were thus investigated and the results are shown in Figure 4. It is obvious that for the samples fabricated with the Meander, Stripe, and Chessboard (5 × 5 mm^2 island size) scanning strategies, the laser-melted tracks are generally evenly and continuously lined up, regularly shaped, and well overlapped with neighboring tracks. There are, however, also some localized regions where the laser-scanned tracks become discontinuous or have poor overlapping with adjacent tracks and, as a result, pores developed there. For the samples made using the Chessboard strategy, pores even form at the boundaries between adjacent islands either due to lack of material filling or poor overlapping (Figure 4(g) through (j)). This is particularly pronounced for the sample made with the Chessboard strategy and with 1 × 1 mm^2 island size, which may have accounted for the highest porosity level of this sample among all the scanning strategies (Figure 3). These pores on the surface of a single layer could remain as internal pores in a bulk sample if they cannot be removed in the subsequent building. The subsequent building, which usually involves not only melting of a fresh powder layer but also partial remelting of the previous layer, offers a chance to engineer the previous layer, *i.e.*, to modify its defects and even microstructure.

To understand the influence of the extent of remelting of the previous layer on the evolution of pores during SLM, the as-fabricated samples were further etched to reveal melt pool development and its influence on porosity distribution within the samples. Figure 5 shows the interaction of solidified melt pools and pores in the samples fabricated with different laser powers or energy densities. At a high laser power, such as 200 W, which gives rise to a high energy density, partial remelting of the previous layer has obviously happened, evidenced by significant overlapping of weld beads from neighboring layers. With sufficient remelting of the previous layer, the interlayer bonding is fairly good. However, there are still some small pores present throughout the sample. Many of them tend to form at two sides of a weld bead or at the triple points of three adjacent solidified melt pools (typically, two from one layer and another from the previous layer); refer to the pores indicated by arrows in Figure 5. This observation was further confirmed by higher-magnification SEM examination results, as shown in Figures 6(a) through (c), where pores that formed at triple points of several adjacent weld beads are clearly demonstrated. Moreover, it is noted that these pores are generally associated with

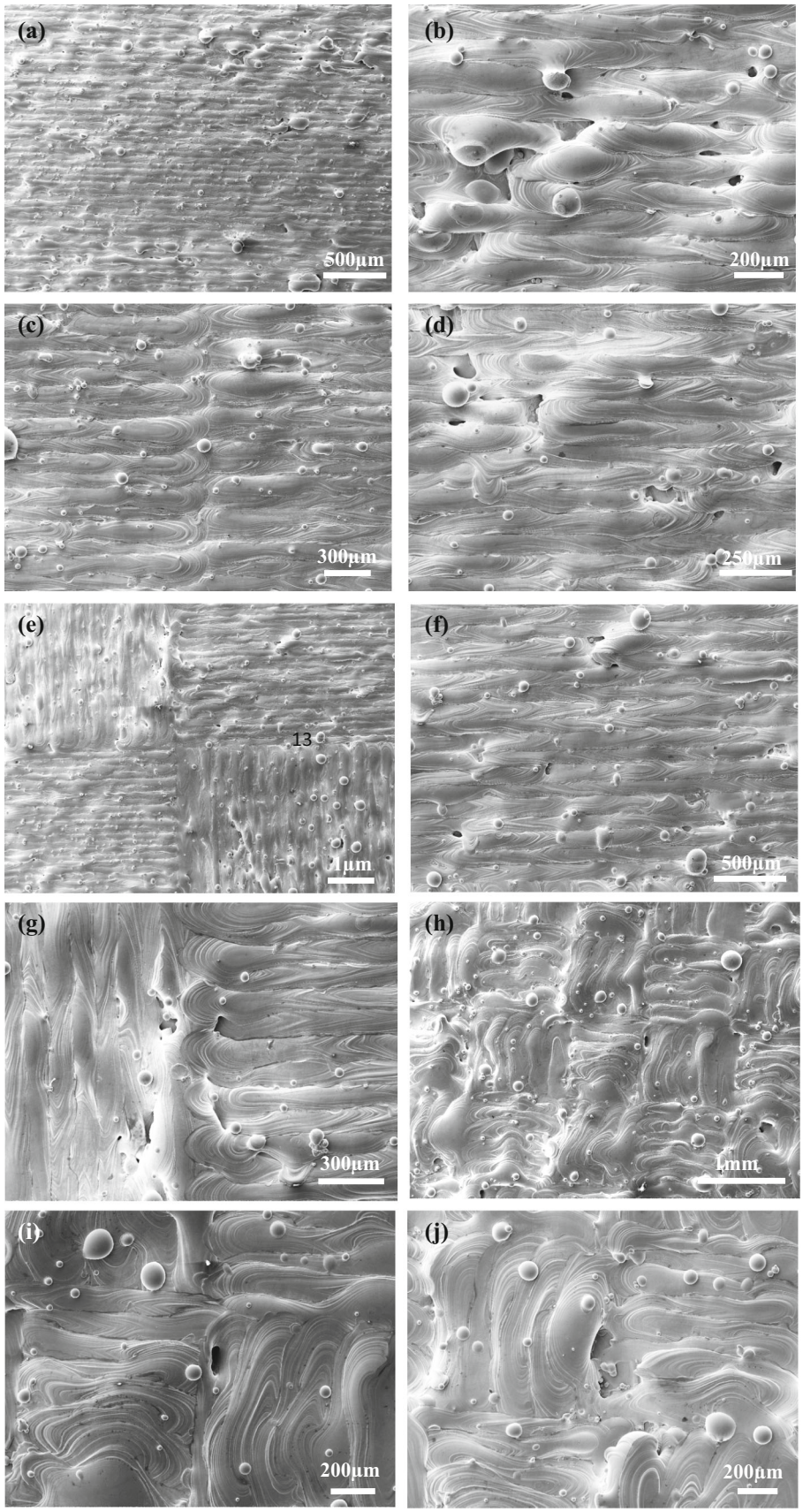

Fig. 4—SEM micrographs showing the top surface structure of samples fabricated at 200 W with varied laser scanning strategies: (*a*) and (*b*) Meander, (*c*) and (*d*) Stripe, (*e*) and (*g*) Chessboard with 5 × 5 mm^2 islands, and (*h*) and (*j*) Chessboard with 1 × 1 mm^2 islands.

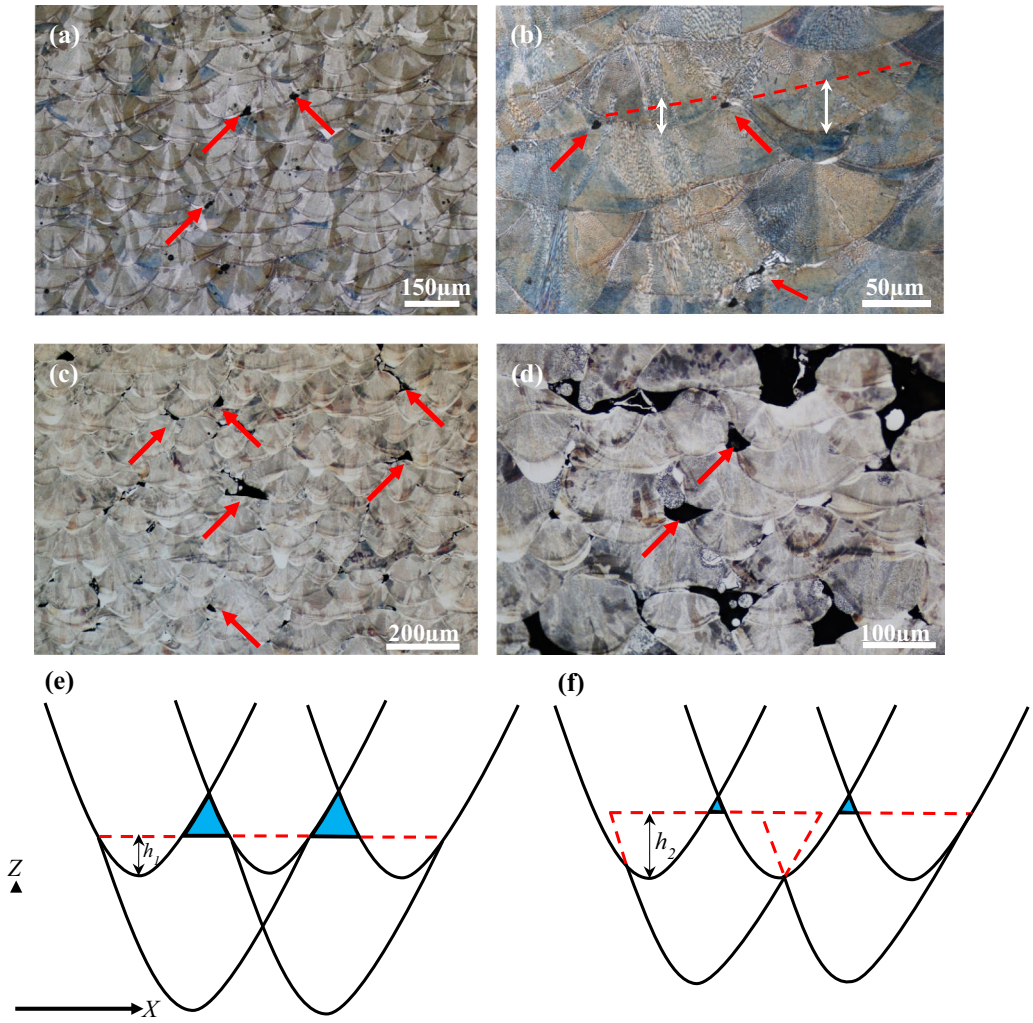

Fig. 5—OM micrographs showing solidified melt pools and porosity distribution within 316L samples fabricated with a Meander scanning strategy under different laser powers: (*a*) and (*b*) 200 W, $E = 48.5$ J/mm^3; (*c*) 140 W, $E = 44.8$ J/mm^3; and (*d*) 110 W, $E = 26.7$ J/mm^3. The single ended arrows show that pores are formed at triple points of several adjacent weld beads and the double ended arrows show the extent of remelting. (*e*) and (*f*) Schematic illustration showing the influence of the extent of remelting (h) or overlapping between two layers on the size of pores developed, $h_2 > h_1$. The blue regions correspond to pores formed at triple points between adjacent weld beads.

those weld beads that have small overlappings with previous layers; *i.e.*, those localized interlayer interfacial areas that show a lesser extent of remelting of previous layers during SLM (Figures 5(a) and (b)). With decreased laser power and decreased energy density, there are an increased number of areas that show insufficient overlapping between adjacent layers (or a lack of remelting of previous layers) and thus an increased number of pores formed at triple points of adjacent solidified weld beads. Moreover, the pores become increasingly larger and irregularly shaped with decreased laser power (Figures 5(b) through (d)). This experimental observation on the relationship between the extent of remelting of the previous layer and pores formed in the samples is further demonstrated in the schematic illustration shown in Figures 5(e) and (f). In general, whenever the energy density is high and there is a larger sufficient remelting of the previous layer, there are fewer and smaller pores, and *vice versa*. When the laser power and energy density are too low (*e.g.*, 110 W), powder particles are not fully melted, as evidenced by the observation of unmelted or partially melted powder particles in Figures 6(d) through (f). These results clearly indicate that reasonably high energy density and sufficient melting of powder particles and remelting of the previous layer are key to interlayer bonding development and minimization of porosity.

To be noted, apart from relatively irregularly shaped pores present between adjacent weld beads, there are also some spherical pores present within solidified melt pools (Figure 5(a)). These pores are generally believed to be due to gas entrapment within melt pools during SLM.

B. *Role of Laser Remelting During SLM*

Based on the above results, it is clear that the extent of remelting of the previous layer shows great influence on interlayer bonding and porosity development in a bulk sample. However, the evolution of pores and surface

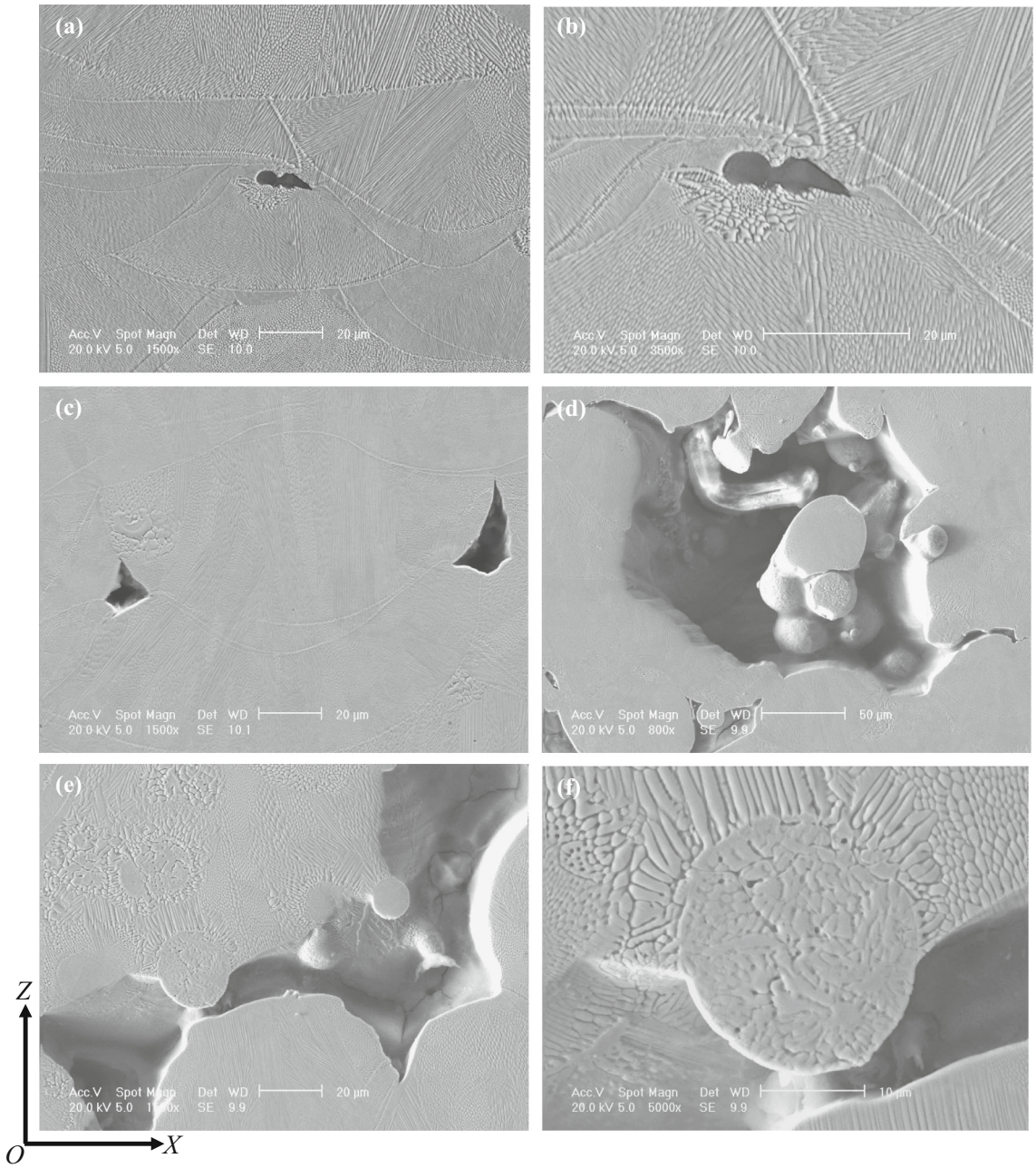

Fig. 6—SEM micrographs showing the morphology and distribution of pores at different laser powers: (*a*) and (*b*) 200 W, $E = 48.5$ J/mm^3; (*c*) 140 W, $E = 44.8$ J/mm^3; and (*d*) through (*f*) 110 W, $E = 26.7$ J/mm^3.

structure during laser remelting is unknown. Therefore, in this section, we discuss the laser remelting experiment that was designed and performed on the uppermost layers of some of the SLM-processed samples (without powder on the uppermost layers). A high laser power of 200 W was used to ensure that the uppermost layers were sufficiently remelted. The remelted layers were then characterized in terms of their surface structure and internal structure. The results are shown in Figures 7 and 8. It is obvious that the uppermost surfaces become much smoother after remelting (in comparison with Figure 4). Even the bumpy surface of the sample fabricated with the Chessboard scanning strategy (1×1 mm^2) was greatly improved after remelting (Figures 4(h) and (d)). More importantly, remelting completely eliminated the open pores present on the uppermost surfaces of SLM-processed samples.

Figure 8 shows the vertical sections of samples fabricated under different laser powers after laser remelting on their uppermost surfaces (without powder particles on them). With remelting, the uppermost layer and previous layer show good bonding. There is almost

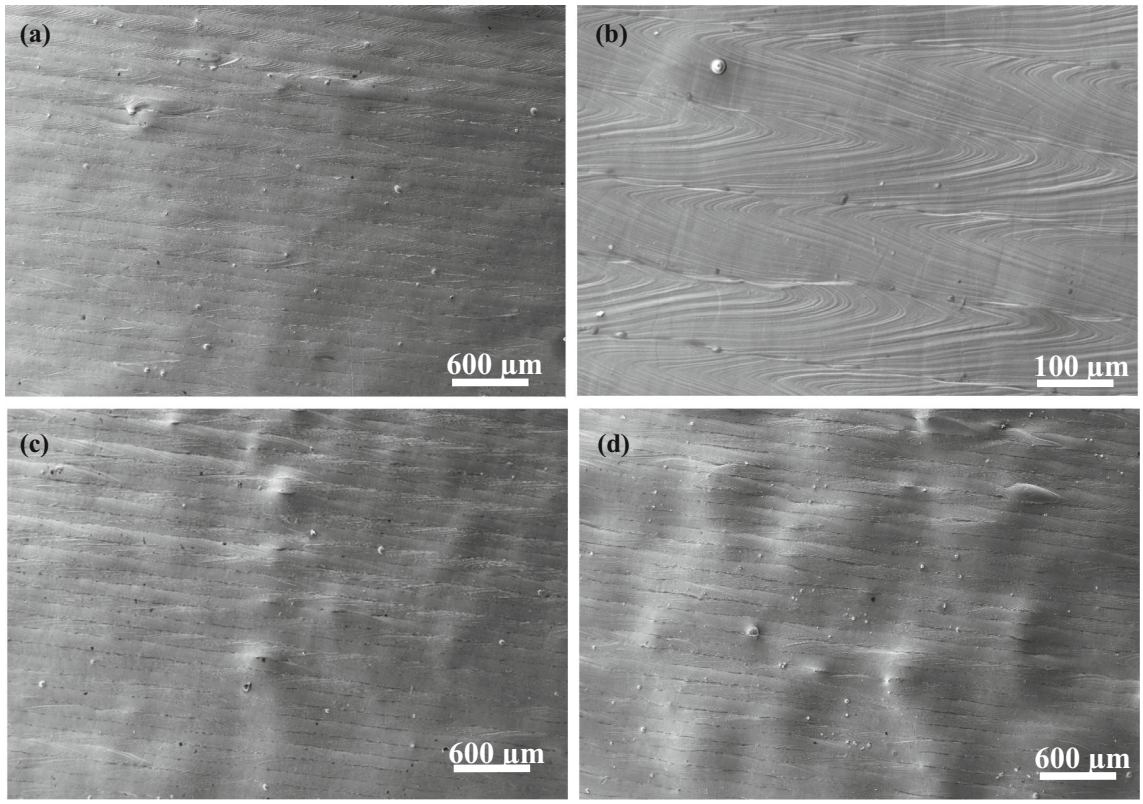

Fig. 7—SEM micrographs showing the top surface structure after laser remelting of the last layers of samples fabricated using different laser scanning strategies: (*a*) and (*b*) Meander, (*c*) Chessboard with 5 × 5 mm^2 islands, and (*d*) Chessboard with 1 × 1 mm^2 islands. The remelting was performed using a 200 W laser beam with a Meander scanning strategy.

no porosity present at the interface between the last two layers of each sample, which is in contrast to the previously built layers where more or less pores at interlayer interfaces can be observed. This is particularly obvious for the sample built with a low laser power (110 W), where many pores formed within the bulk sample, but with a laser remelting on the uppermost surface, the bonding between the remelted layers greatly improved (Figure 8(d)). The improved interlayer bonding *via* laser remelting obviously accounts for the reduced porosity in the bulk samples that was reported in Yasa *et al.*'s work.[7]

To understand the mechanism of how laser remelting affects the development of pores within previous layers, mathematical modeling was conducted. According to Figure 5, there are two types of pores dominant in the current samples: small and spherical pores within solidified melt pools and relatively larger and irregularly shaped pores present between adjacent solidified melt pools. These two types of pores, together with the open pores on the uppermost surfaces of the samples (Figure 4), are modeled in terms of their evolution during remelting. The results are shown in Figure 9. It is shown that the open pores on the uppermost sample surfaces can be quickly removed by the filling of molten material (Stages A1 to A2 in Figure 9(a) or Video 1). As for the spherical pores present within the solidified melt pools, when remelting happens, the pores act differently depending on their gas pressure. High gas pressure pores float up during remelting and, if time allows, will reach the uppermost surface to disappear before solidification (Stages A1 to A4 in Figure 9(a) or Video 1). However, this is a slow mechanism of pore removal, and given the extremely high solidification and cooling rates after SLM melting ($> 10^4$ °C/s), it is likely that most of the gas bubbles could still remain within the bulk materials even after remelting if they are too far away from the uppermost surfaces. In contrast, vacuum pores are much easier to remove, simply through material filling during remelting (Stages B1 to B3 in Figure 9(a) or Video 2). Regarding those pores that are only partially melted during remelting, they will be quickly filled with molten material and closed if they are vacuum (Stages D1 to D3 in Figure 9(b) or Video 3). If they contain gas, they will be compressed by the molten material and become smaller and more spherical (Stages C1 to C3 in Figure 9(b) or Video 4). Given that Marangoni force is not considered in the current modeling, its influence on pore evolution during remelting cannot be demonstrated. However, according to Leung *et al.*'s observation using high speed synchrotron X-ray imaging,[4] the centrifugal Marangoni-driven flow tends to force pores to flow in a clockwise direction, suggesting Marangoni force indeed plays an important role in migration,

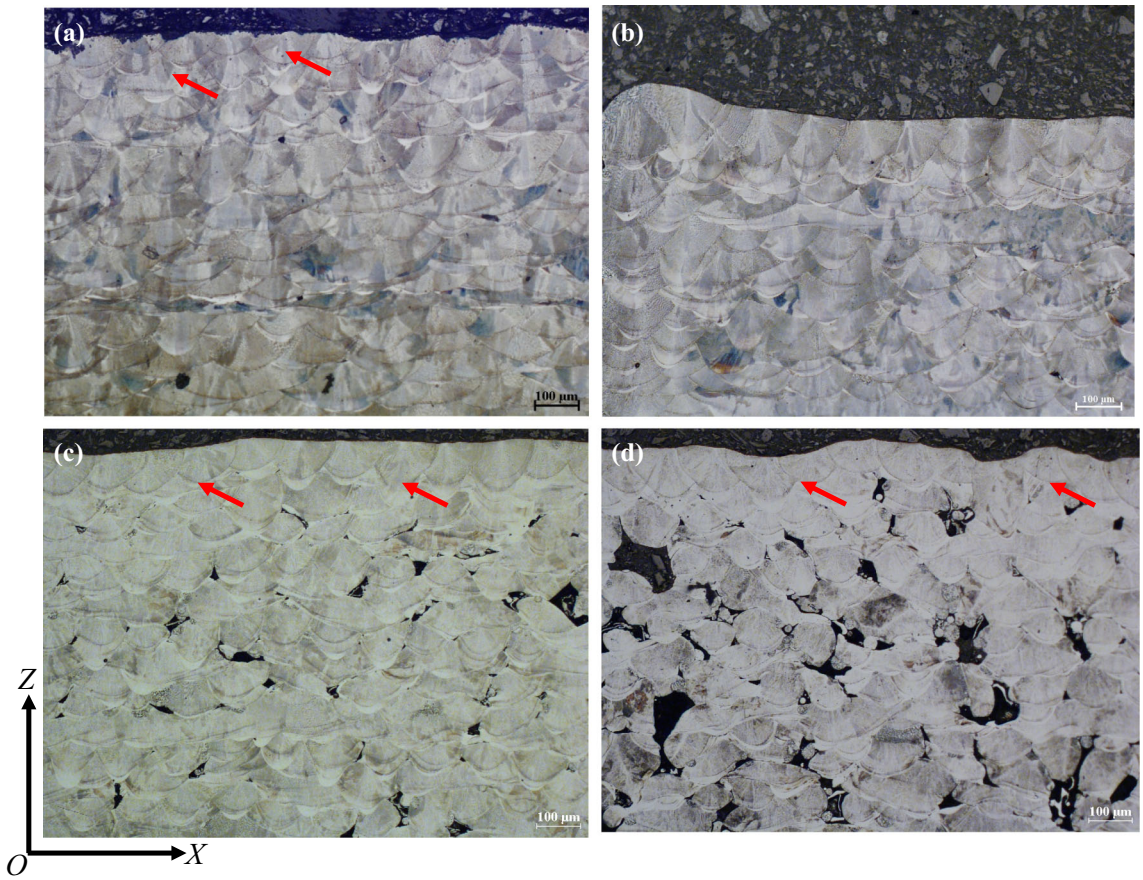

Fig. 8—OM micrographs showing longitudinal sections of the laser remelted layers and a number of previous layers in the samples made with a Meander scanning strategy but at different laser powers: (*a*) 200 W, (*b*) 170 W, (*c*) 140 W, and (*d*) 110 W. The arrows show that the laser remelted layers show good bonding with the previous layer.

dissolution, and dispersion of pores. Future work will focus on the development of improved modeling that will include various forces that can affect melt flow and pore development.

IV. DISCUSSION

The current experimental results clearly demonstrate that the development of surface structure and the formation of pores on a freshly melted layer are highly associated with the melt flow behavior during SLM. Irregularly shaped and rough surface structure and pores are liable to be developed when the melt flow is unstable and discontinuous (Figure 4). This is consistent with previous observations.[1,6,27] The formation of pores within bulk samples, however, turns out to be more related to the extent of remelting of the previous layer or the extent of overlapping between adjacent layers and weld beads since the majority of pores in the current SLM-processed samples were found to be located at triple points of adjacent weld beads or at the interlayer interfaces (Figure 5). With sufficiently high energy density and sufficient remelting of the previous layer during SLM, good bonding between layers together with minimum porosity would be developed. Whenever remelting of the previous layer was insufficient, the overlap between adjacent layers and weld beads became poorer and then an increased number of pores (even elongated pores) were developed in those areas. The processing parameters were found to affect the porosity level in a bulk sample by influencing the extent of remelting of previous layers. Therefore, with decreased laser power and thus decreased energy density, there are an increased number of interlayer interfaces that lack remelting or fusion; as a result, there is an increased number of pores developed in these samples (Figure 5), and *vice versa*. This is believed to be the main reason why the porosity level is so dependent on laser power/energy density. The laser scanning strategy, however, does not greatly affect the input energy density and the extent of remelting of the previous layer, and thus does not affect the porosity level significantly. As such, the laser power/energy density obviously plays a more dominant role than the laser scanning strategy in porosity development during SLM. The current experimental findings are not inconsistent with Tang *et al.*'s geometry-based simulation results, where the depth of overlap between two adjacent layers is believed to be important for porosity

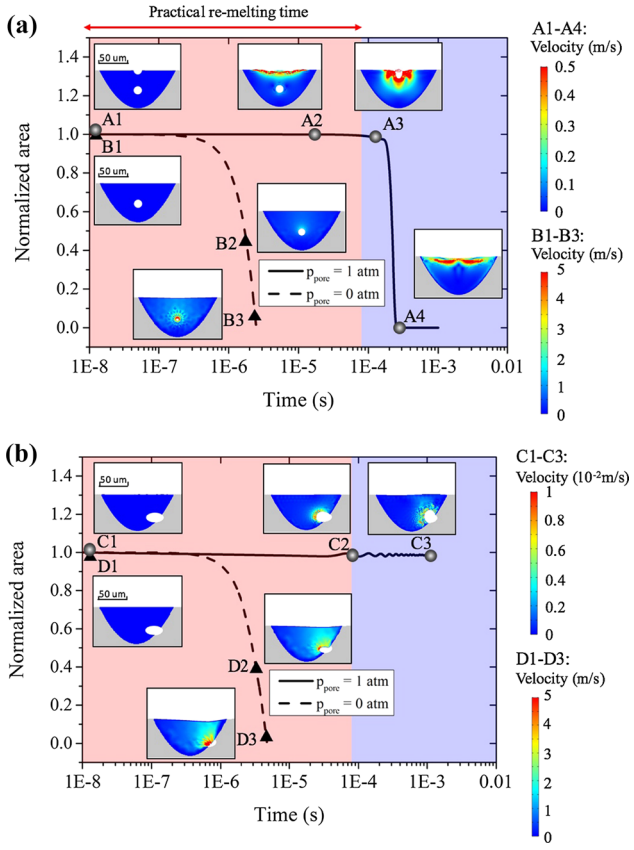

Fig. 9—Morphological evolution and volume variation of pores during remelting: (*a*) pores in a melt pool and (*b*) pores located between a melt pool and its adjacent solid material. Two extreme conditions, one with vacuum pores and the other with pores with a gas pressure of 1 atm, are considered here. A and C represent gas-entrapped pores, while B and D stand for vacuum pores. A1, B1, C1, and D1 correspond to the starting states of different pores in as-fabricated samples; A2, B2, C2, and D2 correspond to the middle of laser remelting; and A3, B3, C3, and D3 correspond to the end of remelting.

development.[28] While a reasonably high laser power is essential for development of good interlayer bonding and minimum porosity in a sample, an excessive laser power may be harmful for porosity development. According to previous studies,[5,6] when a laser power is too high or a laser input energy density is too high, the melt pool can penetrate down through many previous layers and result in the formation of keyhole pores.

Apart from the important role that the extent of remelting plays in the development of pores at interlayer interfacial areas, laser remelting was found to show significant influence on the surface structure and the evolution of pores within a built layer. Both experimental and modeling results show that laser remelting can effectively smooth the rough surfaces and remove the open pores in a newly built layer (Figures 7 and 9(a)). These pores can be easily removed by molten material filling up. Regarding pores within a newly built layer, the pores can be quickly filled up with molten materials and closed if they are vacuum during remelting. For the high gas pressure pores/bubbles, they tend to float up in the remelt pool. For those close enough to the uppermost surface, they stand a good chance of escaping to the surface to disappear, and for those too far from the surface, they may be captured and remain within the layer due to the rapid solidification process after SLM. For partially remelted pores, they are either closed by material filling if they are vacuum or compressed into smaller and more spherical ones if they are filled with gas. Instead of floating up, these pores tend to stay where they were. According to the modeling, the evolution of pores within a new build layer during remelting is governed by several physical forces, including the gravity of molten material, the internal gas pressure and surface tension within the pores, and the thermocapillary force that is induced by the thermal gradient between the surface and bottom of a melt pool. The latter greatly affects the melt flow behavior.

V. CONCLUSIONS

1. Laser power/energy density plays a more dominant role than laser scanning strategy in porosity development within selectively laser-melted 316L samples. To minimize porosity within as-fabricated 316L samples, a relatively high laser power is preferred.
2. The extent of remelting of the previous layer or the overlap between layers dictates the porosity development at interlayer interfaces.
3. Laser remelting effectively smooths rough surfaces and eliminates pores in a newly built layer.
4. The current modeling suggests that open pores on the uppermost layer of a sample and those vacuum pores within samples can be easily removed by remelting, while gas-entrapped pores can only be removed if they can float up to the uppermost surfaces before solidification happens.

ACKNOWLEDGMENTS

The current work was sponsored by the incentive fundings from the School of Engineering, Cardiff University, and the School of Materials Science and Engineering, Beihang University. ZW and LC acknowledge the financial support by the program of the ORAU Ralph E. Powe Junior Faculty Enhancement Award.

ELECTRONIC SUPPLEMENTARY MATERIAL

The online version of this article (https://doi.org/10.1007/s11661-019-05348-0) contains supplementary material, which is available to authorized users.

REFERENCES

1. C.L. Qiu, C. Panwisawas, M. Ward, H.C. Basoalto, J.W. Brooks, and M.M. Attallah: *Acta Mater*., 2015, vol. 96, pp. 72–79.
2. S.A. Khairallah, A.T. Anderson, A. Rubenchik, and W.E. King: *Acta Mater*., 2016, vol. 108, pp. 36–45.
3. M.J. Matthews, G. Guss, S.A. Khairallah, A.M. Rubenchik, P.J. Depond, and W.E. King: *Acta Mater*., 2016, vol. 114, pp. 33–42.
4. C.L.A. Leung, S. Marussi, R.C. Atwood, M. Towrie, P.J. Withers, and P.D. Lee: *Nat. Commun*., 2018, vol. 9, p. 1355.
5. C. Zhao, K. Fezzaa, R.W. Cunningham, H. Wen, F. Carlo, L. Chen, A.D. Rollett, and T. Sun: *Sci. Rep*., 2017, vol. 7, p. 3602.
6. C.L. Qiu, N.J.E. Adkins, and M.M. Attallah: *Acta Mater*., 2016, vol. 103, pp. 382–95.
7. E. Yasa and J.-P. Kruth: *Proc. Eng*., 2011, vol. 19, pp. 389–95.
8. C.L. Qiu, G.A. Ravi, C. Dance, A. Ranson, S. Dilworth, and M.M. Attallah: *J. Alloys Compd*., 2015, vol. 629, pp. 351–61.
9. Z.J. Sun, X.P. Tan, S.B. Tor, and W.Y. Yeong: *Mater. Des*., 2016, vol. 104, pp. 197–204.
10. M.M. Ma, Z.M. Wang, and X.Y. Zeng: *Mater. Sci. Eng. A*, 2017, vol. 685, pp. 265–73.
11. D. Wang, C.H. Song, Y.Q. Yang, and Y.C. Bai: *Mater. Des*., 2016, vol. 100, pp. 291–99.
12. C.L. Qiu, N.J.E. Adkins, and M.M. Attallah: *Mater. Sci. Eng. A*, 2013, vol. 578, pp. 230–39.
13. C.L. Qiu, Y. Sheng, N.J.E. Adkins, M. Ward, H. Hassanin, M.M. Attallah, P.D. Lee, and P.J. Withers: *Mater. Sci. Eng. A*, 2015, vol. 628, pp. 188–97.
14. N. Read, W. Wang, K. Essa, and M.M. Attallah: *Mater. Des*., 2015, vol. 65, pp. 417–24.
15. M.J. Xia, D.D. Gu, G.Q. Yu, D.H. Dai, H.Y. Chen, and Q.M. Shi: *Int. J. Mach. Tools Manuf*., 2017, vol. 116, pp. 96–106.
16. L. Thijs, K. Kempen, J.-P. Kruth, and J.V. Humbeeck: *Acta Mater*., 2013, vol. 61, pp. 1809–19.
17. L. Thijs, F. Verhaeghe, T. Craeghs, J.V. Humbeeck, and J.-P. Kruth: *Acta Mater*., 2010, vol. 58, pp. 3303–12.
18. R. Rashid, S.H. Masood, D. Ruan, S. Palanisamy, R.A. Rahman Rashid, and M. Brand: *J. Mater. Proc. Technol*., 2017, vol. 249, pp. 502–11.
19. S. Catchpole-Smith, N. Aboulkhair, L. Parry, C. Tuck, I.A. Ashcroft, and A. Clare: *Addit. Manuf*., 2017, vol. 15, pp. 113–22.
20. C.L. Qiu, M.A. Kindi, A.S. Aladawi, and I.A. Hatmi: *Sci. Rep*., 2018, vol. 8, p. 7785.
21. B. Chinè and M. Monno: *Proc. 2010 Eur. COMSOL Conf*., Paris, 2010.
22. H.A. Amiri and A.A. Hamouda: *Int. J. Multiph. Flow*, 2013, vol. 52, pp. 22–34.
23. Z. Liu and J.G. Korvink: *Eng. Optimiz*., 2008, vol. 40, pp. 529–58.
24. J. Kim: *Commun. Comput. Phys*., 2012, vol. 12, pp. 613–61.
25. C. Liu and J. Shen: *Physica D: Nonlin. Phenom*., 2003, vol. 179, pp. 211–28.
26. C. Multiphysics, "4.3 User's Guide," 2012.
27. C.L. Qiu, A. Fones, H.G.C. Hamilton, N.J.E. Adkins, and M.M. Attallah: *Mater. Des*., 2016, vol. 109, pp. 98–111.
28. M. Tang, P.C. Pistorius, and J.L. Beuth: *Addit. Manuf*., 2017, vol. 14, pp. 39–48.